Searching for Supersymmetry with the α_T variable in $p\bar{p}$ collisions with the CMS Detector at the Large Hadron Collider

Zoe Hatherell

A thesis submitted in fulfilment of the requirements
for the degree of Doctor of Philosophy
to Imperial College London
December 2011

Contents

Chapter 1

Searching for Supersymmetry with α_T in all-hadronic events

The analysis presented here represents a model-independent search for new physics in the all-hadronic channel, where the final state is defined by the presence of jets and missing energy. Designed to search for signs of supersymmetry whilst remaining sensitive to other new physics models, an inclusive strategy is used imposing restrictions only on the final state. Events are chosen based on their compatibility with a topology of heavy new particles pair-produced in p-p collisions, which decay through a chain with an end product which is stable and undetectable.

Isolating these new physics events from Standard Model background processes is essential in order to identify an excess. Controlling the dominant background from QCD Multijet processed is the central feature of the strategy, implementing use of the powerful discriminant, the α_T variable described in Chapter **??**. The remaining backgrounds from electroweak processes may then be accounted for using data-driven estimation techniques in muon and photon control samples.

1.1   Samples

This analysis uses datasets both from Monte Carlo simulation (MC) and of data recorded by the CMS detector in 2011.

1.1.1   Monte Carlo Simulation

Datasets of simulated events with calculated cross-sections are required for any analysis at the LHC. Due to the hadron-collider nature these rely on the PDF's

Standard Model Background

QCD Multijet

W + jets

Z $\to \nu\bar{\nu}$ + jets

t$\bar{t}$

CMSSM SUSY Signal

For the purpose of understanding the possible yields from CMSSM SUSY, two mSUGRA parameter points are used. CMS has a dedicated set of 10 Low Mass(LM) points designed for initial data-taking from which we have chosen LM4 and LM6, the values of which are found in Table 1.1.

mSUGRA Point	m_0	$m_{1/2}$	A_0	$\tan \beta$	$\text{sign}(\mu)$
LM4	210 GeV	285 GeV	0	10	+
LM6	85 GeV	400 GeV	0	10	+

Table 1.1: The two CMSSM SUSY signal points used and their corresponding mSUGRA parameter values.

These points are chosen for their existence above the exclusion limit set previously, shown in Figure 1.1 on the exclusion plot from the 2010 iteration of this analysis[1].

1.1.2   Data Sample

This analysis considers data collected by CMS at $\sqrt{s} = 7$ TeV in 2011 between March and June, during the data-taking period known locally as Run2011A. Analyses use only the data taken whilst CMS was fully operational, and thus the data used were specified by the certified list of "good runs" that correspond to $1.1 fb^{-1}$ of integrated luminosity.
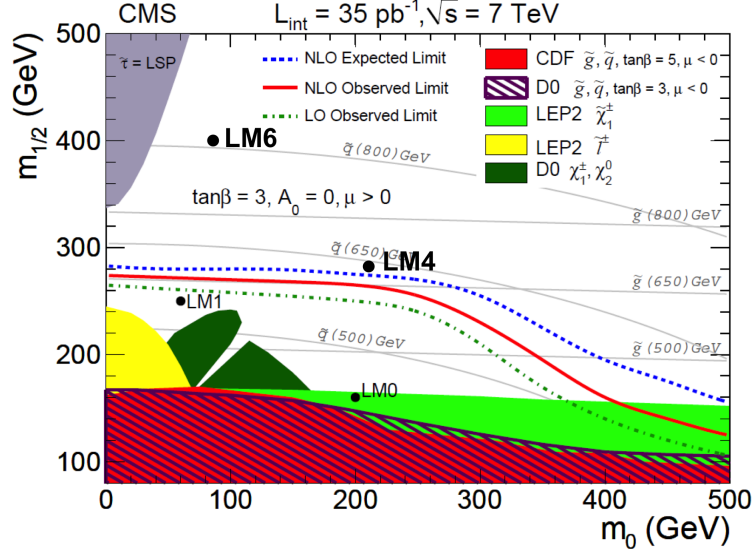
Figure 1.1: The exclusion limit set in the previous incarnation of this analysis with the $35pb^{-1}$ 2010 CMS dataset shown in the $m_0 - m_{1/2}$ plane with $\tan\beta = 10$, $A_0 = 0$ and $sign(\mu) = +$. Reference points LM4 and LM6 to be used in the 2011 analysis are illustrated, in the region yet to be excluded. Previously used reference points LM0 and LM1 are shown below the limit already excluded [1].

As described previously, loose requirements on the types of triggers passed allow the sorting of the data into each Primary Dataset (PD). For the hadronic analysis the HT dataset is used, with basic low-threshold H_T triggers required. Higher threshold triggers are applied subsequently as part of the analysis selection, detailed in Section 1.3.

For the data-driven estimation techniques muon and photon control samples are defined. For the muon control sample, the HT PD is also used, as a low muon p_T requirement makes this better suited than the dedicated Muon PD. However the photon control sample uses the dedicated Photon PD that requires some basic threshold photon triggers to be passed.

1.2 Analysis Framework

For the purpose of the analysis private ntuples are generated fro the RECO samples using the CMSSW framework and CMS's Physics Analysis Toolkit (PAT), retaining all variables from the intermediate step of PAT-tuples recommended by the CMS SUSY group. Followng this private code is used on the ntuples to

perform the analysis.

1.3 Trigger

In order to select the signal events and minimise the contamination from backgrounds, a set of selection criteria is applied. As described previously in Section **??**, data collected by the CMS detector is stored and organised according to the L1 and HLT trigger paths passed. While the datasets chosen in Section **??** have some basic level trigger requirements, we also require a more stringent set of requirements.

In the previous iteration of this analysis for the 2010 dataset, a set of pure H_T triggers was used. However these are unsuitable for the 2011 analysis as due to the increase in instantaneous luminosity the rate of triggers with desirable thresholds have become too high and become prescaled, rendering them unsuitable for the signal selection, although they will play a part in the control region. Moving to higher H_T thresholds is also undesirable as it would reduce a significant portion of the search region.

The use of cross-object triggers is now employed, requiring events that pass thresholds in both H_T and $\not{H}_T$ for the signal region. As the era of data-taking progressed there were several menu-changes, during which time we required the lowest un-prescaled thresholds available at a given time to ensure signal yields are accurate, some of which are implemented in the menu under different versions, the relevant paths appended with `_v*`.

The first set of runs in the 2011 dataset correspond to a trigger used with thresholds in $[H_T, \not{H}_T] = [260,60]$ GeV. After this the CMS standard thresholds were shifted down by 10 GeV, relevant for the major portion of data taking. For all runs henceforth the lowest unprescaled cross-trigger had an H_T threshold of 250 GeV, during which time the $\not{H}_T$ thresholds of the lowest unprescaled evolve through 60, 70 and 90 GeV.

The quantities H_T and $\not{H}_T$ used in the trigger requirements differ from those used in the analysis. The trigger uses jets built in online reconstruction with uncorrected energy to form these quantities, whereas those quantities in our analysis use only jets passing the object requirements and with corrected energy. Thus it is not the case that an H_T trigger of threshold X is efficient for events

HLT Trigger Path
HLT_HT260_MHT60_v2
HLT_HT250_MHT60_v2
HLT_HT250_MHT60_v3
HLT_HT250_MHT60_v4
HLT_HT250_MHT70_v1
HLT_HT250_MHT70_v3
HLT_HT250_MHT70_v4
HLT_HT250_MHT90_v1

Table 1.2: List of HLT trigger paths for the signal selection from which the lowest unprescaled was used or any given run.

with $H_T >$ X in the analysis. It is necessary to ensure the trigger is efficient with regard to analysis cuts in both H_T and $\not{H}_T$.

In this two step process, the efficiencies of pure H_T triggers of thresholds 250 and 260 are identified through comparison to an orthogonal sample, using a Muon H_T cross trigger. These triggers can be considered 100% efficient by an offline H_T cut of 275 GeV, and thus this is selected for the analysis. Having made this cut the efficiency of the $\not{H}_T$ part may be tested, with reference to α_T (which is analogous to a cut on MHT). In the lowest bin of the analysis, $275 < H_T < 325$ GeV a small inefficiency was measured of $0.99^{+0.01}_{0.02}$, and in all other bins $H_T > 325$ the analysis is measured as fully efficient - $1.0^{+0.00}_{-0.03}$.

This analysis makes use of those events which fail the α_T selection criteria also, as the hadronic bulk control sample. In this region the chosen signal triggers would not be efficient as we wish to use the events with low $\not{H}_T$ which would not pass that element of the trigger requirement. Here the pre-scaled H_T triggers are suitable for use, taking into account the prescale factors to gain yields in this bulk sample, an approach which is suitable due to the high statistics from QCD events. The lowest prescale of the trigger thresholds chosen for each H_T bin, shown in Table **??**, are used at each point in the evolution of the trigger menu.

In the muon control sample, due to the low $p_T^\mu = 10$ GeV threshold we use the same triggers as for the hadronic signal sample. The photon sample makes use of the single photon trigger paths shown in Table 1.4, using the lowest unprescaled threshold available for each given run in the data.

Analysis H_T Region	HLT Trigger Paths
$275 < H_T < 325$	`HLT_HT250_v*`, `HLT_HT260_v*`
$325 < H_T < 375$	`HLT_HT300_v*`
$375 < H_T < 475$	`HLT_HT300_v*`, `HLT_HT350_v*`
$475 < H_T < 575$	`HLT_HT440_v*`, `HLT_HT450_v*`
$H_T > 575$	`HLT_HT520_v*`, `HLT_HT550_v*`

Table 1.3: The prescaled HLT trigger paths used for each H_T region of the hadronic control sample, where α_T ¡ 0.55. N.B. The H_T that defines the region is built from jets with corrected energy that pass the requirements of the analysis, while the H_T quoted in the trigger definition is uncorrected and built using online reconstruction jets available to the trigger.

HLT Trigger Paths
`HLT_Photon75_CaloIdVL`
`HLT_Photon75_CaloIdVL_IsoL`
`HLT_Photon90_CaloIdVL`
`HLT_Photon90_CaloIdVL_IsoL`

Table 1.4: The list of HLT trigger paths available used to select the events for the Photon Control sample from which the lowest unprescaled photon threshold is selected in any given run.

Events passing the relevant triggers proceed into the analysis selection.

1.4   Object Definitions

1.4.1   Good Event Definition

In order for an event to be considered suitable for use in physics analyses, it must be defined as a "Good Event". Such an event is required to have at least one non-fake good primary vertex with $N_{dof} > 4$. Constraints on the vertex position along the beam axis $|z_{vtx}| < 24$ cm and perpendicular to the axis of $\rho < 2$ cm must be satisfied. Events that have many fake tracks are identified as monster events and removed, by requiring that the ratio of High Purity tracks to the total number be greater than 25% in events with more than 9 tracks.

1.4.2   Jets

The jets used in this analysis are Calo Jets, reconstructed as described in Section ?? using the anti-k$_T$ jet clustering algorithm. In addition, a reconstructed jet must pass an additional selection in order to be considered for the analysis:

- Corrected jet transverse momentum requirement of $p_{\mathrm{T}}> 50$ GeV

- Jet pseudo-rapidity $|\eta| < 3$ required to ensure within the fiducial range of the calorimeter systems.

- Passes "loose" jet identification criteria to reject jets resulting from unphysical energy using cuts in Table 1.5.

Any jet which passes the E_{T} and η requirements but fails the "loose" identification criteria is noted, and the event is marked as containing an "odd" jet, as the presence of such a particle reflects an event whose kinematics are poorly understood and may therefore lead to a misleading $\not{H}_{\mathrm{T}}$.

1.4.3 H_T and $\not{H}_{\mathrm{T}}$

The calculation of both H_T and $\not{H}_{\mathrm{T}}$ is performed using only the jets selected by the selection above in Section 1.4.2.

Definition	Variable	Cut
Fraction of jet energy contributed by the "hottest" hybrid photo-diode	f_{HPD}	< 0.98
Minimum number of cells required to contribute 90% of the jet energy	N_{cells}^{90}	≤ 2
Fraction of jet energy contributed by deposits in ECAL	f_{EM}	> 0.01
Balance of the energy measured in the short(E_S) and long(E_L) HF fibers.	$R_{HF} = \frac{(E_S - E_L)}{(E_S + E_L)}$ (if $p_T^{jet} > 80$ GeV)	$R_{HF} > -0.9$ ($-0.9 < R_{HF} < 1$)

Table 1.5: *Set of cuts applied in "loose" CaloJet ID used to reject jets resulting from fake calorimeter deposits representing unphysical energy. Devised using cosmic run data as a pure sample of non-collider "fake" jets, full details of which can be found in [2]*

1.4.4 Muons

Although muons are not required by the analysis, a veto on them must be employed, based on muons that satisfy the following set of criteria:

- $p_T^{\mu} > 10$ GeV

- $|\eta| < 2.5$

- Relative Combined Isolation $= (Iso_{tracker} + Iso_{ECAL} + Iso_{HCAL})/p_T^{\mu} < 0.15$[1]

- Passes "tight" muon identification, using cuts shown in Table 1.6.

1.4.5 Electrons

Similarly electrons are also defined for veto purposes, with the definition of an electron in the analysis as that passing the following cuts:

- $E_T^e > 10 GeV$

- $|\eta| < 2.5$

---

[1]The components $Iso_{tracker}(Iso_{ECAL}, Iso_{HCAL})$ represent the sum of $p_T(E_T)$ in the relevant detector component, calculated in a cone of R = 0.3 in $\eta - \phi$ around there muon trajectory. The track hits used to reconstruct the muon are not used and any muon deposit in the calorimeters is removed via a smaller veto cone.

Definition	Variable	Cut
Reconstructed with outside-in algorithm	Global Muon	Required
Reconstructed with inside-out algortithm	Tracker Muon	Required
Global muon track fit quality	χ^2	< 10
Number of hits in the silicon tracker included in track	N_{trk}^{hits}	> 10
Number of pixel hits in N_{trk}^{hits}	N_{pixel}^{hits}	> 0
Number of hits in muon system included in Global Muon	N_{muon}^{hits}	≥ 1
Transverse impact parameter with respect to vertex	d_{xy}	< 2 mm

Table 1.6: Set of cuts applied in "tight" Muon ID, taken from [3]

- Combined Isolation $= (\sum_{tracker} p_T + \sum_{ECAL} E_T + \sum_{HCAL} E_T)/p_T^e < 0.15$

- Pass WP95 electron identification implemented using cuts in Table 1.7.

Definition	Variable	Barrel Cut	End-Cap Cut
RMS of the width in η of the crystals about the most energetic crystal in the seed	$\sigma_{i\eta i\eta}$	< 0.01	< 0.03
Difference in ϕ between track and supercluster	$\Delta\phi_{vtx}$	< 0.8	< 0.7
Difference in η between track and supercluster	$\Delta\eta_{vtx}$	< 0.007	< 0.01
Ratio of HCAL energy in $\Delta R = 0.15$ to ECAL seed energy	H / E	< 0.15	< 0.07

Table 1.7: Set of cuts applied in "WP95" Electron ID, taken from [4] corresponding to an intended 95% efficiency for signal electrons in W events for electrons with $p_T > 20$ GeV.

1.4.6 Photons

Photons in the analysis are defined by the following set of requirements:

---

[1]where electron $p_T > 20$ GeV, measured with a sample of $W \to e$ events.

- $p_T^\gamma > 25$ GeV

- $|\eta| < 2.5$

- Passes "tight" photon cut-based identification (including isolation) using cuts shown in Table 1.8.

Definition	Variable	Barrel Cut	End-Cap Cut
Tracker Isolation in a cone of R=0.4	Iso_{trk}	$< (2.0 GeV + 0.001 E_T^\gamma)$	
ECAL Isolation in an outer cone of R=0.4 (inner cone R=0.06 removed).	Iso_{ECAL}	$< (4.2 GeV + 0.006 E_T^\gamma)$	
HCAL Isolation in an outer cone of R=0.4 (inner cone R=0.15 removed).	Iso_{HCAL}	$< (2.2 GeV + 0.0025 E_T^\gamma)$	
RMS of the width in η of the crystals about the most energetic crystal in the seed	$\sigma_{i\eta i\eta}$	< 0.013	< 0.030
Ratio of HCAL energy in $\Delta R = 0.15$ to ECAL seed energy	H / E	< 0.05	< 0.05

Table 1.8: Set of cuts applied in "tight" Photon ID, taken from [5]

1.5 Pre-Selection

A basic selection of events used for comparison of distributions between data and monte-carlo events shall be known as "pre-selection", following the details set out in this section.

HCAL Barrel and End-cap (HBHE) Noise Fiter Events where noise has been identified in the HCAL are removed also, using an algorithm which checks for Photodetectors which have at east 17 out of 18 channels with an E > 1.5 GeV.

Following these conditions events are then selected by the following criteria, using the definitions of physics objects according to the criteria stated previously:

- Pass triggers as detailed in Section 1.3.

- Pass Good Event selection as detailed in Section 1.4.1.

- Require events with $N_{jet} \geq 2$

- $N_{muon} = N_{electron} = 0$ to reduce the effects of missing energy from neutrinos.

- $N_{photon} = 0$ to ensure a pure hadronic set of events.

- Events with > 0 "odd" jets are vetoed.

- Additional constraint on the transverse momentum of the two leading jets $p_T^{j1}, p_T^{j2} > 100$ GeV.

- Additional constraint on the leading jet pseudorapidity $|\eta^{j1}| < 2.5$.

- $H_T \geq 275$ GeV

1.6 Final Signal Selection

After the preselection a final set of cuts is applied, including the α_{T} cut that defines the signal region alongside cleaning cuts which remove events that may lead to inaccurate results.

- $\alpha_{\mathrm{T}} > 0.55$

- If the ratio $R_{miss} = \not{H}_{\mathrm{T}} / \not{E}_{\mathrm{T}} > 1.25$, the event is rejected. This protect the quantity α_{T} from the scenario where many jets fail the $p_T = 50$ GeV threshold thus resulting in fake $\not{H}_{\mathrm{T}}$ and thus misleading values of α_{T}.

- To prevent against fake missing energy resulting from dead or masked cells in the ECAL or the gap between the barrel and end-caps the following procedure is used: The jet most likely to be responsible for the $\not{H}_{\mathrm{T}}$ is found. If the angle ϕ between this jet and the vector $\vec{\not{H}}_{\mathrm{T}}$ (known as $\Delta\phi*$) less than 0.5 then the $\eta - \phi$ distance between the jet and the nearest masked ECAL cell is computed, along with the distance from the detector gap. If either distance is smaller than 0.3 then the event is rejected.

1.7 An H_T Shape Analysis

Previous iterations of this analysis strategy with the 35pb^{-1} 2010 LHC dataset [1] used a cut-and-count strategy for all events passing the selection, defining the

signal region by an $H_T > 375$ and using lower regions in H_T as control regions. The 2011 analysis follows the same selection but motivated by the increasing luminosity is undertaken as a Shape Analysis in bins of H_T, using the whole range $H_T >275$ GeV as a signal region. This allows greater sensitivity to states of higher mass.

The set of lower bin edges are as follows: [275,325,375,475,574,675,775,875], where each bin is exclusive with an upper limit corresponding to the lower edge of the next bin, except in the case of the final bin which is inclusive $H_T >875$. The background estimation techniques employed from data therefore are designed to identify the contribution in each distinct bin.

In order to include the two lowest bins in H_T is is necessary to scale the jet thresholds stated in Section **??** in order to maintain even event kinematics allowing a shape analysis approach. The background from $t\bar{t} +$ jets carries a bias to higher jet multiplicities compared to the other EWK components, and thus with identical jet definitions exhibits a turn on behaviour in H_T. In order to remedy this, the lowest two bins have both the p_T threshold required by definition and the additional second jet p_T requirement scaled. The scale factor is $l/375$. where l represents the bin lower edge in question, leading to the thresholds shown in Table 1.9.

H_T Region	Jet Definition	Second-Leading Jet Cut
$275 < H_T < 325$	$p_T > 36.7$ GeV	$p_T^{j1}, p_T^{j2} > 73.3$ GeV
$325 < H_T < 375$	$p_T > 43.3$ GeV	$p_T^{j1}, p_T^{j2} > 86.7$ GeV
$H_T > 375$	$p_T > 50$ GeV	$p_T^{j1}, p_T^{j2} > 100$ GeV

Table 1.9: The three different regions of jet scaling, with values indicated both for the basic definition of a jet used in the analysis, and the second-to-leading jet energy cut. The former is especially important as this alters the value of H_T as this is calculated using the jets in the event.

1.8 Data to Monte-Carlo Comparisons

Distributions of the 2011 data with MC samples alongside are shown in this section. The MC samples are normalised to 1.1fb^{-1} for shape comparison and to illustrate the accuracy of modelling provided, although these are not used in

background estimation as data control samples are used later.

In Figure 1.2 distributions of H_T, the jet multiplicity (NJet) and α_T are shown for events that pass the pre-selection with an additional cut of $\not{H}_T > 100$ GeV to ensure trigger efficiency. For simplicity only bins with $H_T > 375$ GeV have been included in the plots, so as to maintain one set of jet thresholds. There is good agreement in all three variables. Figure 1.2(c) shows the high discriminatory power of the α_T variable between the QCD "fake" $\not{E}_T$ background and signal events with real $\not{E}_T$. The region $0.46 < \alpha_T < 0.6$ is expended in Figure 1.2(d), illustrating the rapid QCD fall-off to zero that motivates the chosen cut value of 0.55.

The distributions of jet multiplicity, $\Delta\phi^*$ and M_{eff} after the final selection cuts are applied can be seen respectively in Figure **??**. Data shows a good overall comparison to the Standard Model MC, although here statistics are more limited accounting for fluctuations. The $\Delta\phi^*$ distribution in Figure **??** is consistent with the expectation that the α_T cut completely eradicate contamination from QCD events, as any evidence of such would lead to a peak at low values, instead of the flat behaviour seen. In addition no notable excess can be seen of data over MC although this observation is merely an aside, as a more detailed shape analysis will be used to evaluate this quantitatively in later sections.
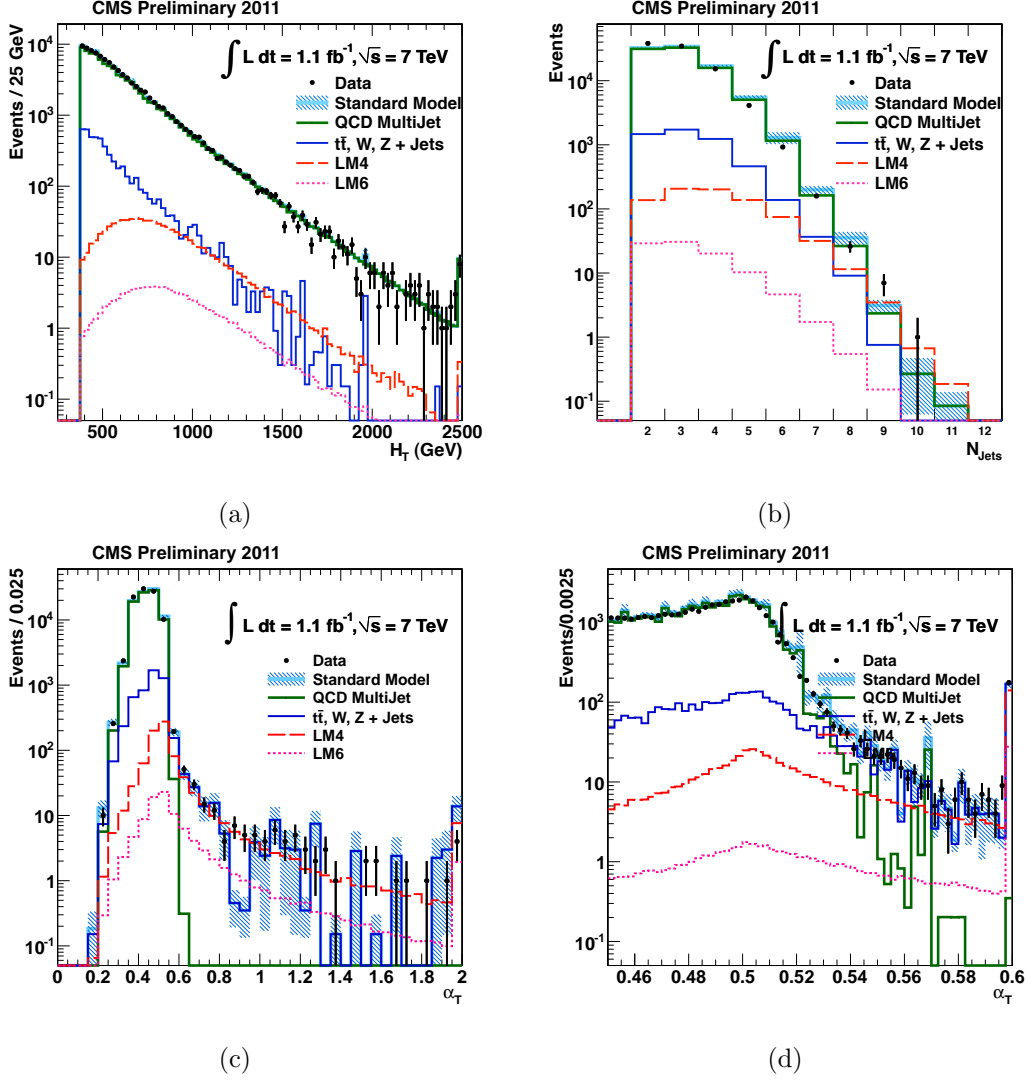
Figure 1.2: Distributions of (a) H_T, (b) NJet, (c) α_T showing comparisons of 1.1 fb^{-1} 2011 7TeV CMS Data and equivalently weighted Monte-Carlo prior to the α_T selection cut, for $H_T \geq 375$ GeV and $\not{H}_T > 100$ GeV. The α_T distribution is also shown zoomed (d) in the region $0.46 < \alpha_T < 0.6$. SUSY Signal reference points LM4 & LM6 shown for illustration of potential yields.
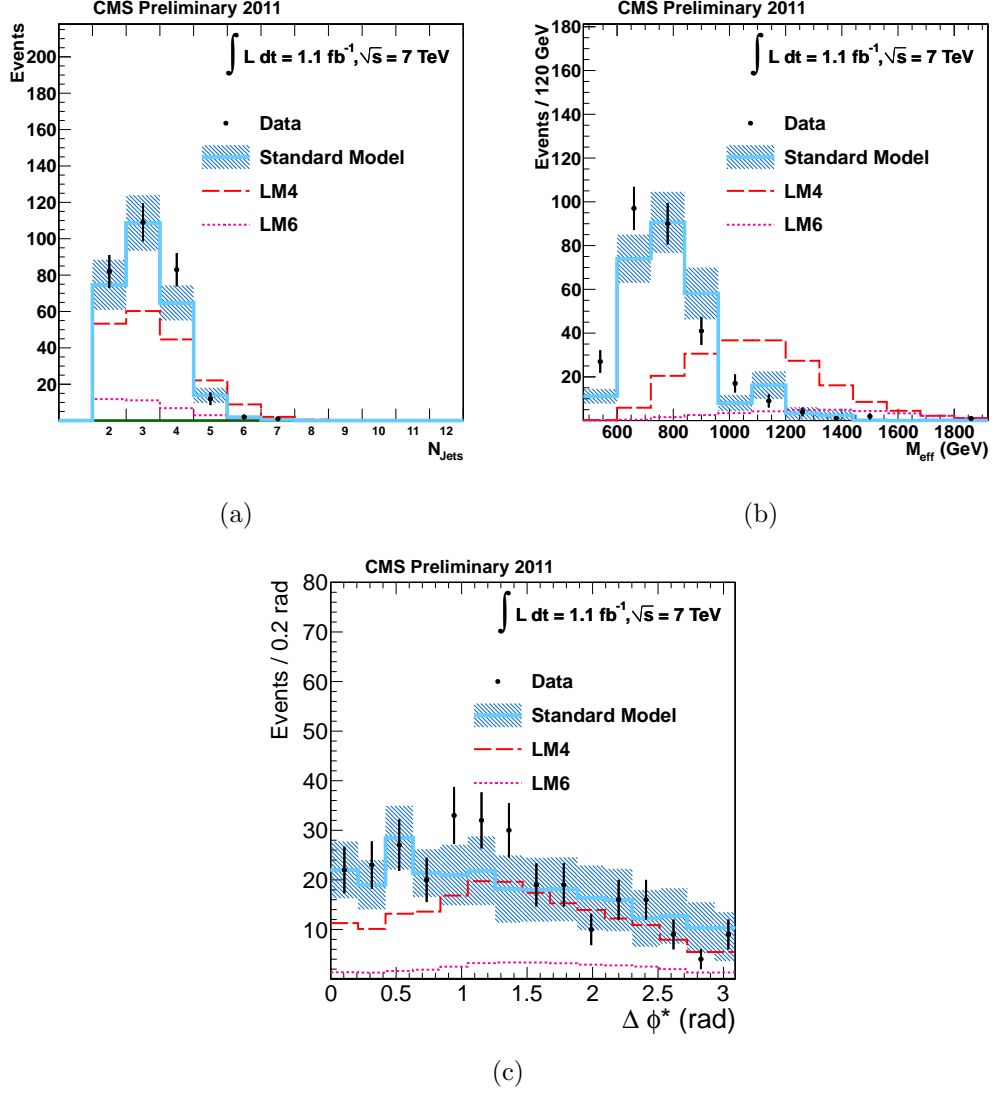
(a)

(b)

(c)

Figure 1.3: Distributions of (a) Jet Multiplicity, (b) M_{eff} ($= H_T + \not{H}_T$) and (c) $\Delta\phi^*$ showing comparisons of 1.1 fb^{-1} 2011 7TeV CMS Data and equivalently weighted Standard Model Monte-Carlo in basic kinematic quantities after the full α_T selection. SUSY Signal reference points LM4 & LM6 shown for illustration of potential yields.
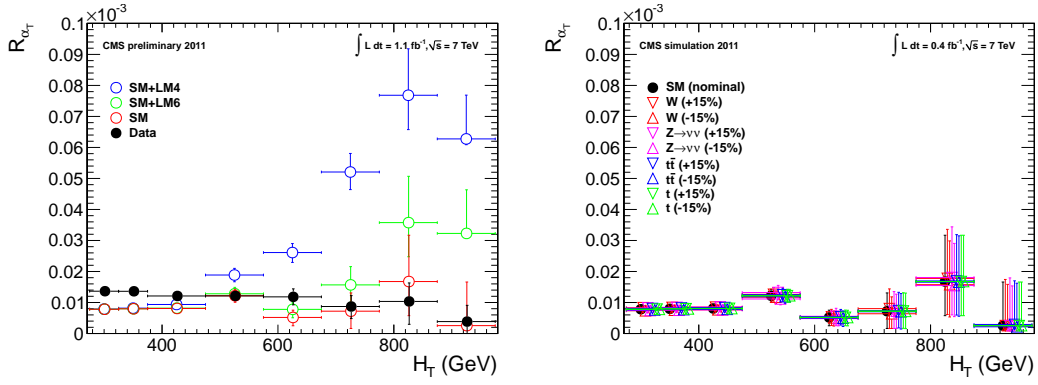
Figure 1.4: (Left) The dependence of R_{α_T} on H_T for events with $N_{\text{jet}} \geq 2$. (Right) Dependence of rat on H_T when varying the effective cross-section of the four major EWK background components individually by ±15%. (Markers are artificially offset for clarity.)

1.8.1 Dependence of R_{α_T} on H_T

1.9 Data-Driven Background Estimation

1.9.1 Total background prediction

1.9.2 Estimating EWK background using high p_T using W+Jets events

Types of decay contributing to Muon Control Sample

1.9.3 Estimation Z $\nu\bar{\nu}$ + jets background using photon + jets events

1.10 Systematic Uncertainties

1.11 Simultaneous Fit

1.12 Limits

1.13 Conclusion

(a)

(b)

(c)

(d)

(e)

(f)
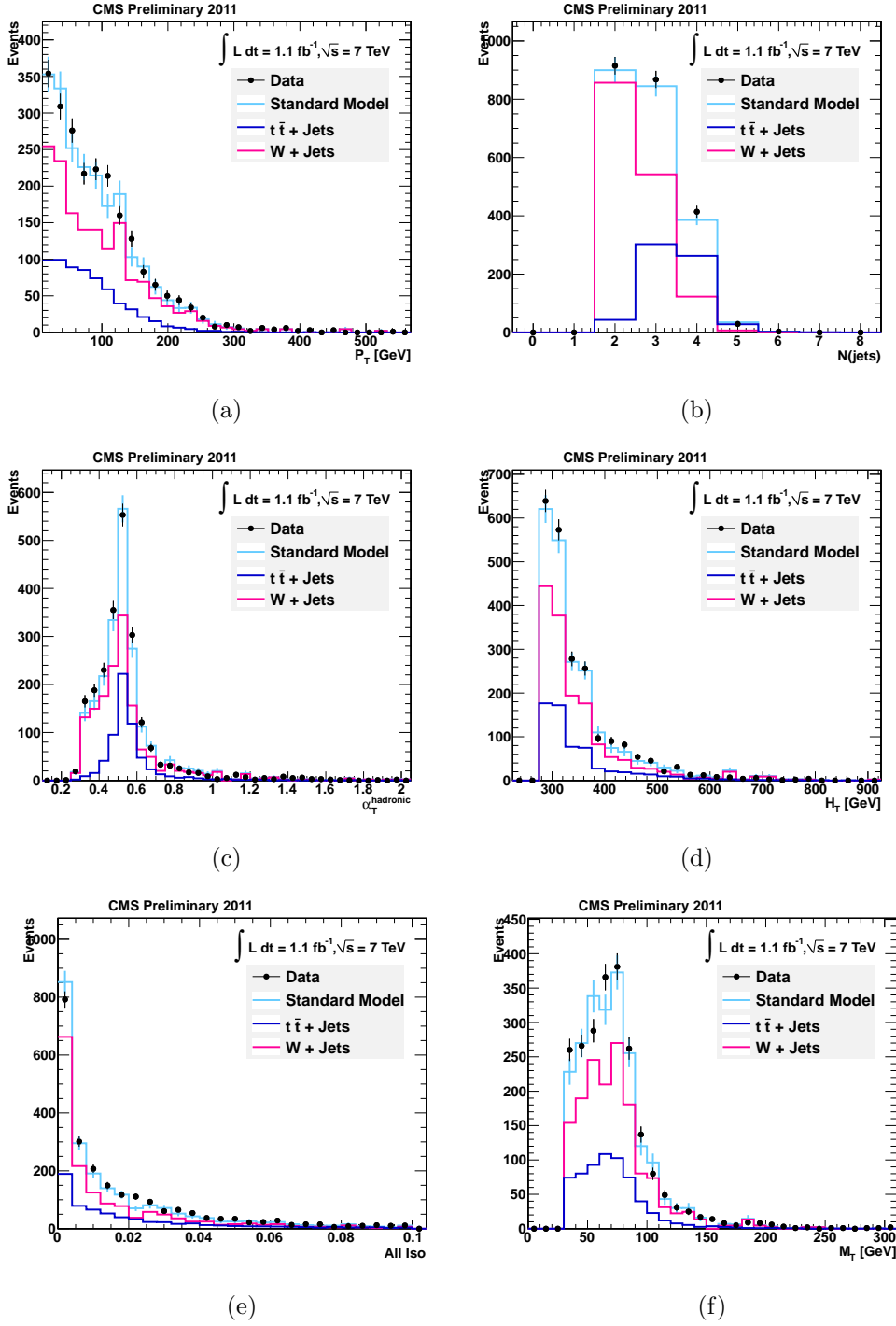
Figure 1.5: Data - Monte Carlo comparisons for the muon control selection before the $\alpha_T > 0.55$ cut is applied, shown for (a) α_T and (b) H_T, (c) Muon Combined Isolation and (d) M_T. A cut of HT > 375 *GeV has been applied, to select the region of fixed jet thresholds.*
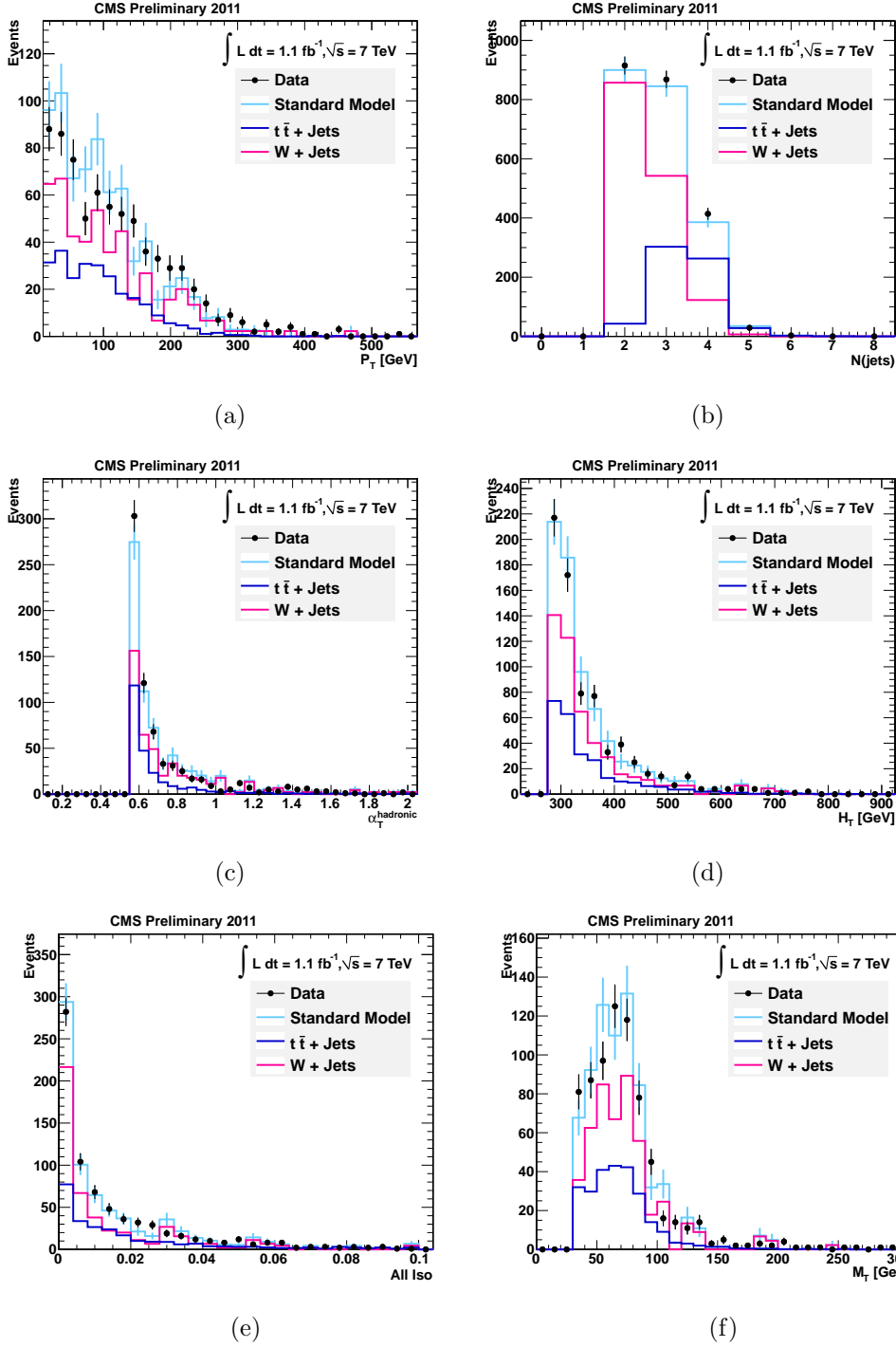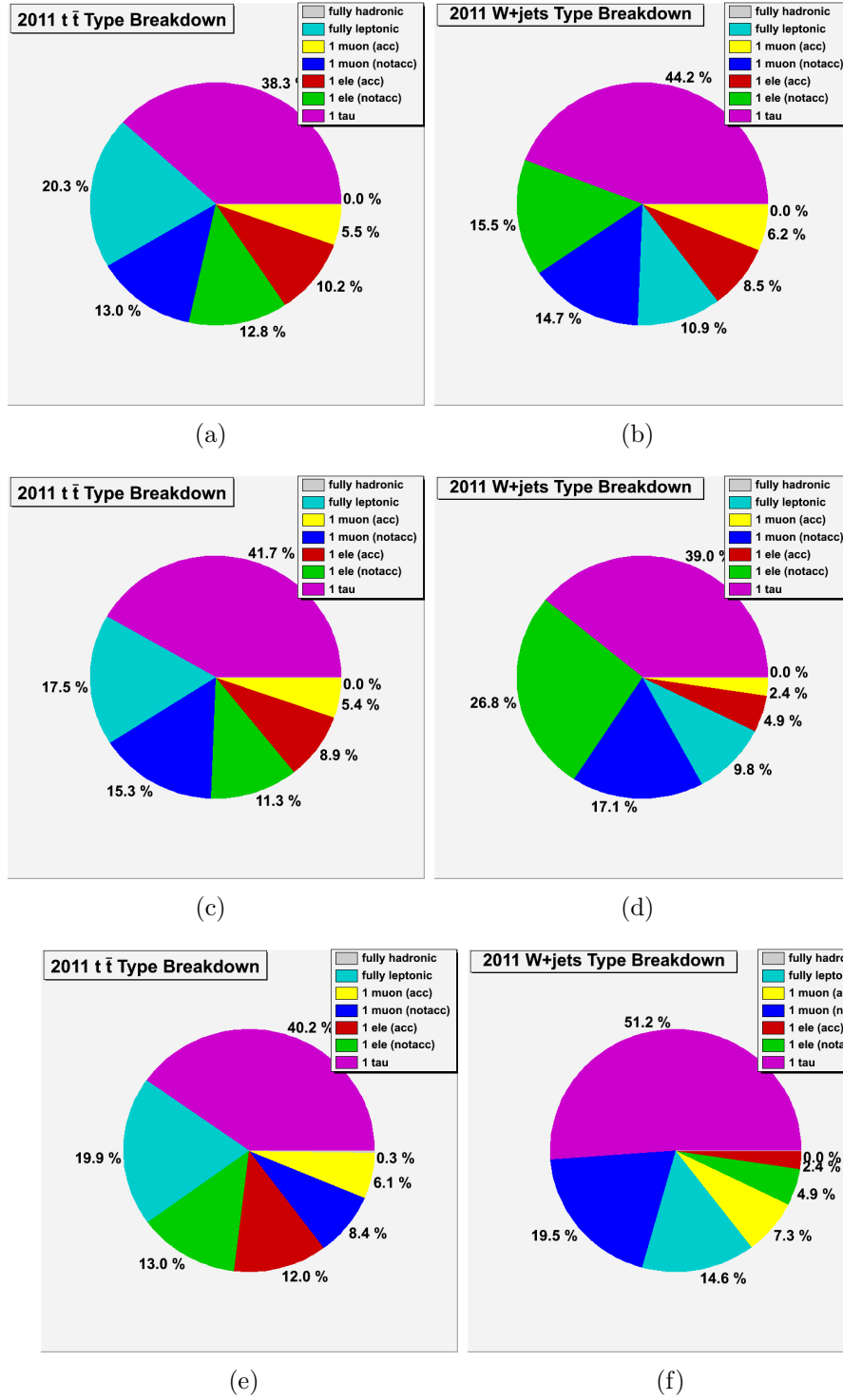
Figure 1.6: Data - Monte Carlo comparisons for the muon control selection after the $\alpha_T > 0.55$ cut is applied, shown for (a) H_T and (b) M_T, (c) Muon Combined Isolation and (d) M_T. A cut of $\mathrm{HT} > 375$ GeV has been applied, to select the region of fixed jet thresholds.

Figure 1.7: Type breakdown of decays resulting in an event selected by the Muon Control selection, shown using Monte-Carlo truth information separately for $\mathrm{t\bar{t}}+$ jets (left) and $\mathrm{W}+$ jets (right) events. The breakdown is made separately for each jet-scale case: $275 < H_T < 325$ GeV (top), $325 < H_T < 375$ GeV (middle), and $H_T > 375$ GeV (bottom).
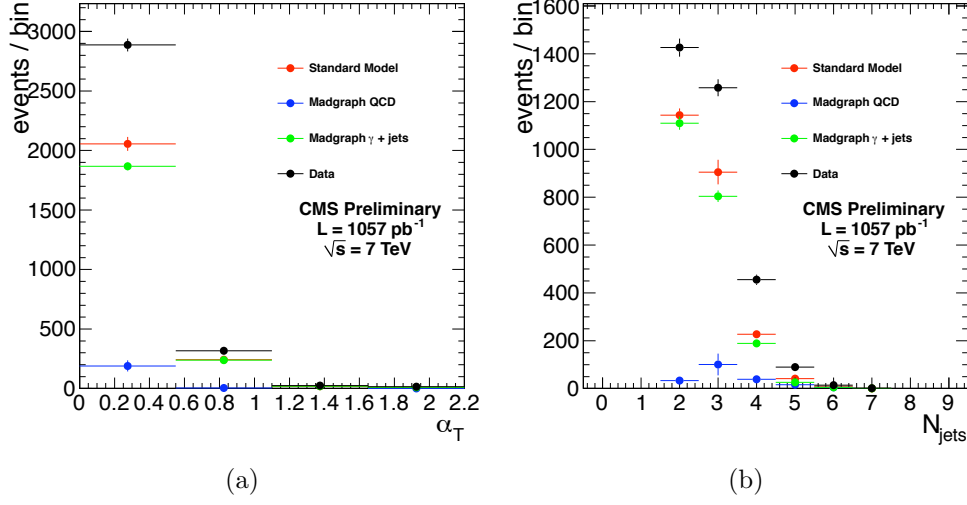
Figure 1.8: Data-MC comparisons for the photon control sample. $H_T > 375$ GeV and $\cancel{H}_T/H_T > 0.4$ are required. Left: the distribution of α_T. Right: the distribution of the number of jets.
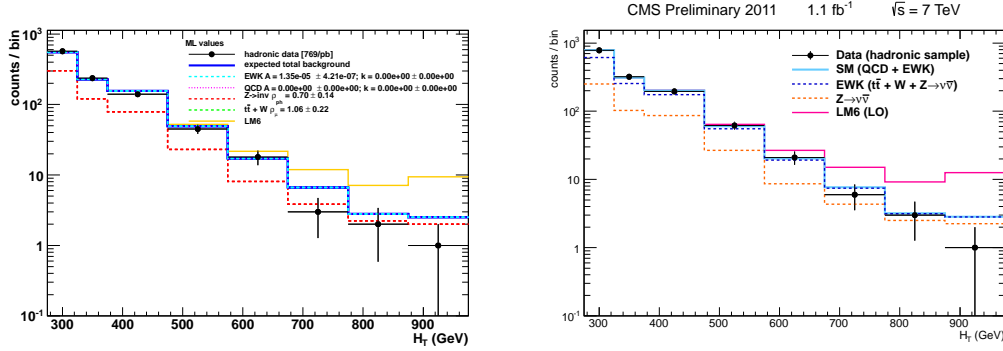

Figure 1.9: H_T distribution for events in the hadronic signal sample for scenario a) (left) and scenario b) (right). Shown are the events observed in data (black points), the outcome of the fit (blue line) and a breakdown of the individual background contributions as predicted by the control samples. A possible signal contribution from benchmark point LM6 is indicated as well (yellow line).
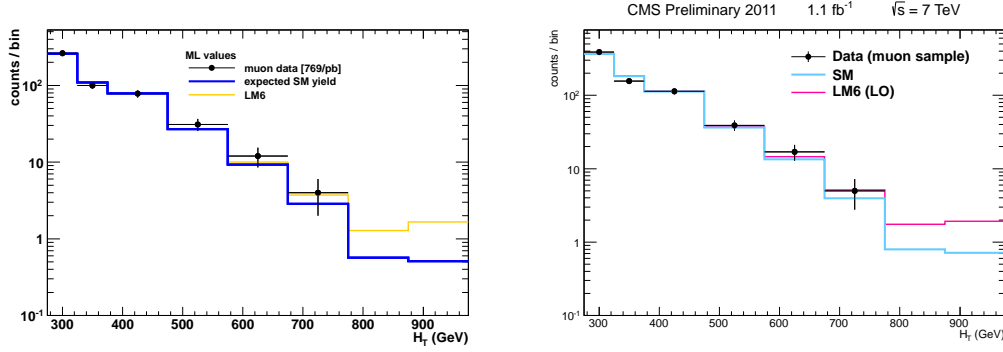
Figure 1.10: H_T distribution for events selected in the muon control sample for scenario a) (left) and scenario b) (right). Shown are the events observed in data (black points), the outcome of the fit (blue line) and the MC expectation (dashed line). A possible signal contribution from benchmark point LM6 is indicated as well (yellow line).
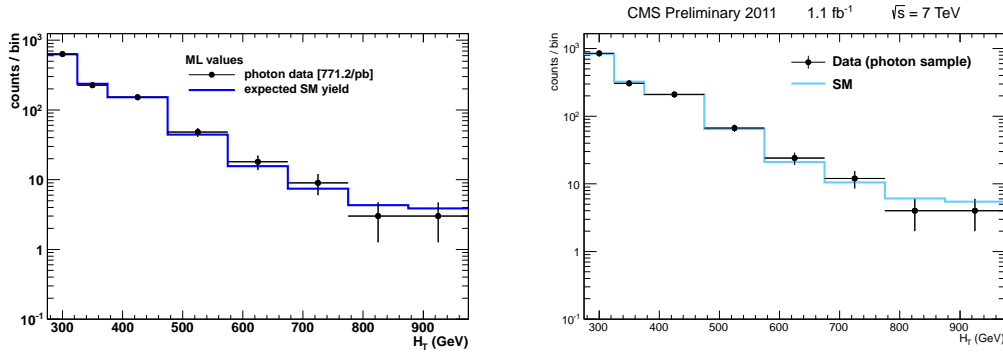

Figure 1.11: H_T distribution for events selected in the photon control sample for scenario a) (left) and scenario b) (right). Shown are the events observed in data (black points), the outcome of the fit (blue line) and the MC expectation (dashed line).
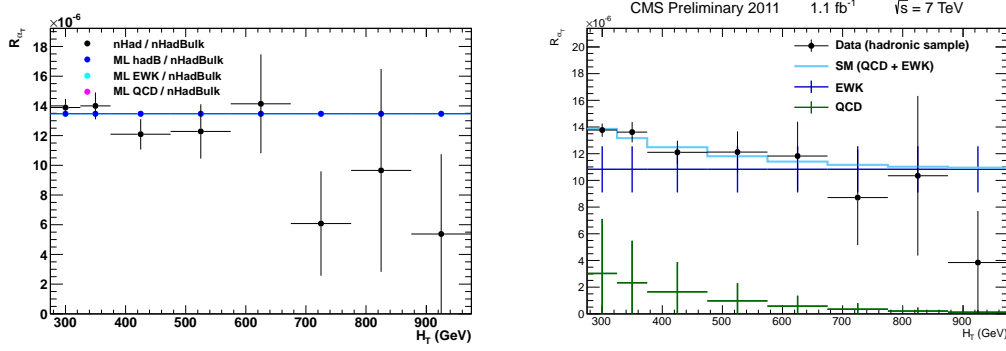
Figure 1.12: R_{α_T} as a function of H_T as observed in data (black points) and the results of the fit assuming different scenarios: a) (left) and b) (right) .
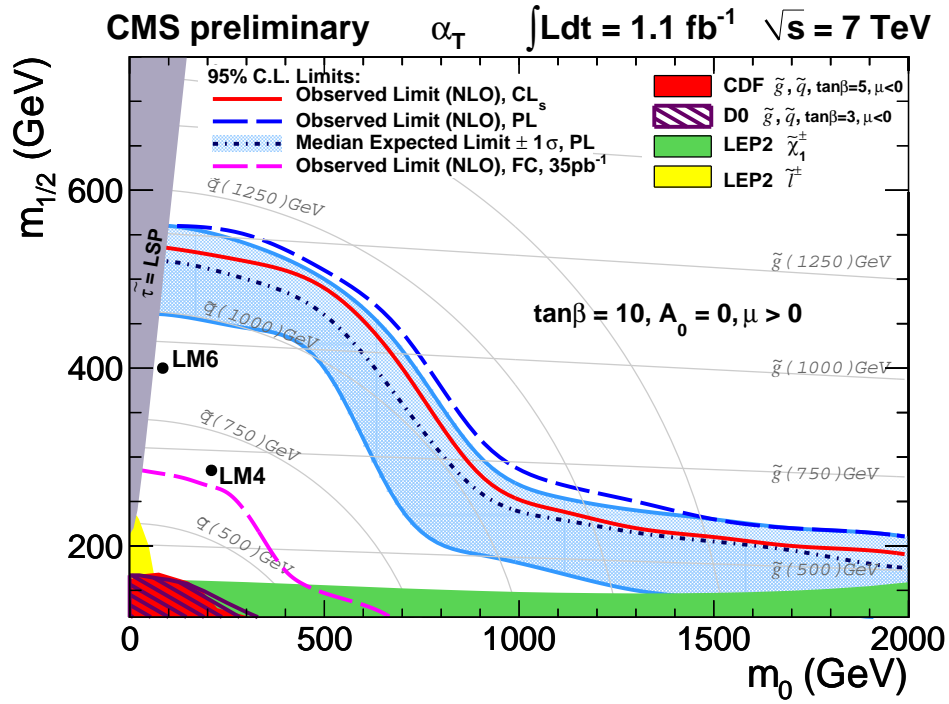

Figure 1.13: Observed and expected 95% CL exclusion contours in the CMSSM $(m_0, m_{1/2})$ plane $(\tan\beta = 10, A_0 = 0, \mu > 0)$ using NLO signal cross sections using the Profile Likelihood (PL) method. The expected limit is shown with its 68% CL range. The observed limit using the CL_s method is shown as well.

Appendix A

HT 1.1fb^{-1} Data

```
/HT/Run2011A-May10ReReco-v1/AOD
/HT/Run2011A-PromptReco-v4/AOD
```

Photon 1.1fb^{-1} Data

```
/Photon/Run2011A-May10ReReco-v1/AOD
/Photon/Run2011A-PromptReco-v4/AOD
```

Standard Model Background Monte Carlo

```
/QCD_Pt_*_TuneZ2_7TeV_pythia6/Spring11-PU_S1_START311_V1G1-v1/AODSIM
/QCD_TuneD6T_HT-*_7TeV-madgraph/Spring11-PU_S1_START311_V1G1-v1/AODSIM
/TTJets_TuneZ2_7TeV-madgraph-tauola/Spring11-PU_S1_START311_V1G1-v1/AODSIM
/TToBLNu_TuneZ2_*-channel_7TeV-madgraph/Spring11-PU_S1_START311_V1G1-v1/AODSIM
/WJetsToLNu_TuneZ2_7TeV-madgraph-tauola/Spring11-PU_S1_START311_V1G1-v1/AODSIM
/ZinvisibleJets_7TeV-madgraph/Spring11-PU_S1_START311_V1G1-v1/GEN-SIM-RECO
/GJets_TuneD6T_HT-40To100_7TeV-madgraph/Spring11-PU_S1_START311_V1G1-v1/AODSIM
```

SUSY Signal Reference Monte Carlo

```
/LM4_SUSY_sftsht_7TeV-pythia6/Spring11-PU_S1_START311_V1G1-v1/AODSIM
/LM6_SUSY_sftsht_7TeV-pythia6/Spring11-PU_S1_START311_V1G1-v1/AODSIM
```

Bibliography

[1] Vardan Khachatryan et al. "Search for Supersymmetry in pp Collisions at 7 TeV in Events with Jets and Missing Transverse Energy". *Phys.Lett.*, **B698** (2011) 196–218, 1101.1628.

[2] The CMS Collaboration. "Calorimeter Jet Quality Criteria for the First CMS Collision Data". **CMS-PAS-JME-09-008**.

[3] The CMS Collaboration. "Performance of muon identification in pp collisions at $\sqrt{s} = 7$ TeV". **CMS-PAS-MUO-10-002**.

[4] N. Adam et al. "Measurements of Inclusive W and Z Cross Sections in pp Collisions at $\sqrt{s} = 7$ TeV". **CMS AN 2010/116**.

[5] The CMS Collaboration. "Isolated Photon Reconstruction and Identification at at sqrt(s) = 7 TeV". **CMS-PAS-EGM-10-006**.